MCB
Journals.ASM.org

# Dynamics of Mitochondrial DNA Nucleoids Regulated by Mitochondrial Fission Is Essential for Maintenance of Homogeneously Active Mitochondria during Neonatal Heart Development

**Takaya Ishihara,[a] Reiko Ban-Ishihara,[a] Maki Maeda,[a,b] Yui Matsunaga,[b] Ayaka Ichimura,[a] Sachiko Kyogoku,[c] Hiroki Aoki,[d] Shun Katada,[e] Kazuto Nakada,[e] Masatoshi Nomura,[f] Noboru Mizushima,[b,g] Katsuyoshi Mihara,[a,h] Naotada Ishihara[a,b]**

Department of Protein Biochemistry, Institute of Life Science, Kurume University, Kurume, Japan[a]; Department of Physiology and Cell Biology, Tokyo Medical and Dental University, Tokyo, Japan[b]; Department of Medicine, Division of Cardiovascular Medicine, Kurume University School of Medicine, Kurume, Japan[c]; Cardiovascular Research Institute, Kurume University, Kurume, Japan[d]; Faculty of Life and Environmental Sciences, University of Tsukuba, Ibaraki, Japan[e]; Department of Medicine and Bioregulatory Science, Kyushu University, Fukuoka, Japan[f]; Department of Biochemistry and Molecular Biology, Graduate School and Faculty of Medicine, The University of Tokyo, Tokyo, Japan[g]; Department of Molecular Biology, Graduate School of Medical Science, Kyushu University, Fukuoka, Japan[h]

**Mitochondria are dynamic organelles, and their fusion and fission regulate cellular signaling, development, and mitochondrial homeostasis, including mitochondrial DNA (mtDNA) distribution. Cardiac myocytes have a specialized cytoplasmic structure where large mitochondria are aligned into tightly packed myofibril bundles; however, recent studies have revealed that mitochondrial dynamics also plays an important role in the formation and maintenance of cardiomyocytes. Here, we precisely analyzed the role of mitochondrial fission *in vivo*. The mitochondrial fission GTPase, Drp1, is highly expressed in the developing neonatal heart, and muscle-specific Drp1 knockout (Drp1-KO) mice showed neonatal lethality due to dilated cardiomyopathy. The Drp1 ablation in heart and primary cultured cardiomyocytes resulted in severe mtDNA nucleoid clustering and led to mosaic deficiency of mitochondrial respiration. The functional and structural alteration of mitochondria also led to immature myofibril assembly and defective cardiomyocyte hypertrophy. Thus, the dynamics of mtDNA nucleoids regulated by mitochondrial fission is required for neonatal cardiomyocyte development by promoting homogeneous distribution of active mitochondria throughout the cardiomyocytes.**

Mitochondria not only produce energy by oxidative phosphorylation but also play critical roles in metabolism and cellular signaling. Mitochondrial morphology is regulated by a balance between fusion and fission, and recent studies have shown that the dynamic features of mitochondria are also important for cellular processes such as apoptosis, reactive oxygen species (ROS) production, $Ca^{2+}$ signaling, mitochondrial quality control, and tissue differentiation (1–3). Mitochondrial fusion is regulated by GTPases such as Mfn1, Mfn2, and OPA1. Mitochondrial fusion factors Mfn2 and OPA1 have been isolated as gene products causal of neurodegenerative disorders such as Charcot-Marie-Tooth neuropathy and autosomal dominant optic atrophy, respectively. Analysis of these mitochondrial fusion factors also revealed a role of intermitochondrial communication in the maintenance of uniformly active mitochondria (4, 5). Mitochondrial fusion is also important for mitochondrial DNA (mtDNA) homeostasis, as deficiency of mitochondrial fusion factors in cultured cells and skeletal muscle results in reduced mtDNA copy numbers and accumulation of mtDNA mutations (6) for unknown reasons. Mitochondrial fission is regulated by the dynamin-related GTPase protein Drp1; however, the physiological role of mitochondrial fission remains poorly understood, especially *in vivo*. We and other groups have previously reported that Drp1 is essential for embryonic and neonatal development, as well as neuronal function in humans and mice (7–10).

In mammalian mitochondria, multicopy mtDNA assembles with DNA binding proteins such as TFAM to form nucleoid structures (11, 12). We recently reported that mitochondrial fission defects, but not fusion defects, cause altered nucleoid structures in cultured cells: nucleoids in Drp1-deficient cells tend to be highly aggregated in hyperfused crista-rich mitochondria, designated mito-bulbs (13). However, the physiological role of nucleoid morphology remains unknown.

Mitochondria are highly enriched in and dispersed throughout the cytoplasm of cardiomyocytes in the heart to guarantee a sustainable energy supply by oxidative phosphorylation (14, 15). As mitochondria become tightly packed into myofibril bundles, they tend to lose their morphological dynamics (16–18). However, recent research has demonstrated that factors involved in mitochondrial dynamics also participate in heart function. Heart-specific Mfn1/2 double-knockout (DKO) mice showed lethality by heart failure, exhibiting respiratory dysfunction and mitochondrial fragmentation/swelling (19, 20). Mfn2 also helps recruit the Parkinson's disease-related E3 ubiquitin ligase Parkin to mitochondria in the heart via phosphorylation by PINK1 (PTEN-induced putative kinase protein 1). Defects in this process lead to

**Received** 26 August 2014 **Returned for modification** 28 September 2014
**Accepted** 21 October 2014

**Accepted manuscript posted online** 27 October 2014

**Citation** Ishihara T, Ban-Ishihara R, Maeda M, Matsunaga Y, Ichimura A, Kyogoku S, Aoki H, Katada S, Nakada K, Nomura M, Mizushima N, Mihara K, Ishihara N. 2015. Dynamics of mitochondrial DNA nucleoids regulated by mitochondrial fission is essential for maintenance of homogeneously active mitochondria during neonatal heart development. Mol Cell Biol 35:211–223.
doi:10.1128/MCB.01054-14.

Address correspondence to Naotada Ishihara, ishihara_naotada@kurume-u.ac.jp.



doi:10.1128/MCB.01054-14

mitophagy deficiency that results in accumulation of abnormal mitochondria (21). Mitochondrial fission is also important for heart function, as a point mutation in mouse Drp1 causes cardiomyopathy (22). Further, other roles of mitochondrial fission were analyzed by RNA interference (RNAi), expression of the dominant negative form of Drp1 in cultured cardiomyocytes, or administration of Drp1 inhibitor Mdivi-1 to mice, which revealed that the ablation of mitochondrial fission can have protective effects against stress caused by hypoxia and ischemia-reperfusion (23, 24). However, the detailed molecular mechanisms and roles of mitochondrial fission *in vivo*, especially in the developing heart, remain to be revealed.

Here, we analyzed mice that are deficient in mitochondrial fission in muscles and found critical roles for the appropriate distribution of mtDNA during heart development. Mitochondrial fission plays important roles in the formation of highly organized myofibrils and maintenance of uniformly active mitochondria with mtDNA nucleoids in cardiomyocytes.

## MATERIALS AND METHODS

**Materials.** The following commercial antibodies were used in the present study: mouse monoclonal anti-Drp1 (8/DLP1; BD Transduction), anti-cytochrome *c* (6H2.B4; BD Transduction), anti-OPA1 (18/OPA1; BD Transduction), anti-β-actin (AC74; Sigma-Aldrich), anti-α-actinin (EA-53; Sigma-Aldrich), anti-LC3B (L7543; Sigma-Aldrich), anti-Parkin (P6248; Sigma-Aldrich), anti-DNA (AC-3010; Progen), anti-COX1 (1D6E1A8; Abcam), MitoProfile Total Oxphos Rodent WB antibody cocktail (ab110413; Abcam), anti-Mfn1 (3C/9; Abnova), anti-HSP60 (SPA-807; Stressgen), rabbit monoclonal anti-glyceraldehyde-3-phosphate dehydrogenase (anti-GAPDH) (14C10; Cell Signaling), rabbit polyclonal anti-Tom20 (SC-11415; Santa Cruz Biotechnology), anti-Ki-67 (ab15580; Abcam), anti-cleaved caspase-3 (9661; Cell Signaling), anti-Fis1 (ALX-210-907; Alexis); anti-Mff (17090-1-AP; Proteintech), and goat polyclonal anti-LaminB (SC-6216; Santa Cruz Biotechnology). Polyclonal antibodies against Tom40 and Tim44 used here were described previously (7). Alexa Fluor 488-, 568-, or 660-labeled goat anti-mouse IgG, IgG1, IgG2a, or IgM or anti-rabbit IgG and horseradish peroxidase (HRP)-conjugated anti-mouse or anti-rabbit IgG (Molecular Probes), anti-mouse kappa (1050-05; SouthernBiotech) or anti-goat IgG (SC-2020; Santa Cruz Biotechnology) was used as a secondary antibody. Hoechst 33258 and rhodamine-phalloidin were purchased from Molecular Probes. The target sequences of the RNAi oligonucleotides (Bonac Corporation, Kurume, Japan) were as follows: 5′-GCGCAGAACUCUA GCUGUA-3′ for mouse Drp1, 5′-ACUCAAAGCUCUUAAGAAA-3′ for mouse Mfn1, 5′-GGAAGAGCACCGUGAUCAA-3′ for mouse Mfn2, and 5′-UACUAUUCGACACGCGAAG-3′ for the negative control.

**Mice.** Drp1-conditional-knockout mice have been described previously (7). To generate conditional Drp1-deficient mice, Drp1 floxed mice ($Drp1^{flox/flox}$) were crossed with transgenic (Tg) mice expressing Cre recombinase. Tg mice expressing Cre under the control of the muscle creatine kinase (Mck) promoter were used to produce muscle-specific (MS) Drp1-KO mice ($Drp1^{flox/flox}$; Mck-Cre). Mouse experiments were performed in accordance with the guidelines of the animal ethics committee of Kurume University.

**Isolation of neonatal mouse cardiomyocytes.** The heart ventricle was excised from neonatal mice, and cardiomyocytes were isolated as previously described (25). In brief, cardiomyocytes were isolated from postnatal day 1 (P1) or P2 neonate mice and cultured on laminin-coated coverslips at 37°C under 5% $CO_2$ in Dulbecco's modified Eagle medium (DMEM)–F-12 medium (Wako, Japan) supplemented with 20% fetal bovine serum (Sigma-Aldrich, St. Louis, MO), 5% horse serum (Life Technologies, Carlsbad, CA), 1 μg/ml insulin (Wako), 20 μm cytosine-β-D-arabinofuranoside (Sigma-Aldrich), and penicillin-streptomycin (Nacalai, Japan). In the knockdown (KD) experiments, cardiomyocytes were cultured for 24 h or 96 h after cell isolation and then small interfering RNAs (siRNAs) were transfected into the cells using Lipofectamine RNAiMax (Life Technologies) according to the manufacturer's instructions.

**Immunofluorescent analysis.** For immunofluorescence staining, mouse heart was perfused with Ringer's solution, fixed in 1% paraformaldehyde for 1 h, embedded in OCT compound, and frozen in liquid nitrogen. These blocks were cut to a thickness of 5 μm using a CM3050S cryostat (Leica). For staining of Ki-67 and cleaved caspase-3, sections were treated with citrate buffer at 56°C for 30 min for antigen retrieval. Sections were permeabilized with 0.1% Triton X-100 in phosphate-buffered saline (PBS) for 10 min and then blocked by 5% bovine serum albumin (BSA) in PBS for 30 min. The sections were incubated with primary antibodies overnight at 4°C, washed with PBS, and incubated with secondary antibodies for 45 min at room temperature. For staining of F-actin, rhodamine-phalloidin was incubated together with secondary antibodies. Immunofluorescence microscopy of primary cardiomyocytes was performed as described previously (13). Briefly, cells grown on coverslips were fixed with 4% paraformaldehyde, permeabilized with 0.2% Triton X-100, stained with primary antibodies, and then visualized with secondary antibodies. Samples were observed under a Zeiss LSM700 confocal microscope with a Plano Apochromat 63×/1.4-numerical-aperture oil immersion objective. Confocal images were acquired using Zeiss ZEN 2010LSM software.

**Histochemical staining.** Fresh-frozen sections obtained using a CM3050S cryostat were treated with succinate dehydrogenase (SDH) or cytochrome *c* oxidase (COX) histochemical stain and then stained with hematoxylin-eosin as described previously (26). COX staining for electron microscopy samples was done as described previously (26). For COX staining of primary cultured cardiomyocytes, cells were fixed in 4% paraformaldehyde for 15 min at room temperature, rinsed in PBS twice for 5 min each, incubated in cytochrome oxidase staining solution (0.6 mg/ml diaminobenzidine, 0.3 mg/ml cytochrome *c*, and 45 mg/ml sucrose in 0.1 M phosphate buffer) for 1.5 h at 37°C, and rinsed twice for 5 min in 0.1 M Tris buffer (pH 8.0).

**Echocardiography.** Echocardiographic studies were performed using a Vevo770 ultrasonograph (VisualSonics) equipped with an RMV703 scanhead under general anesthesia, as described previously (27). Interventricular septal thickness (IVST), left ventricular posterior wall thickness (PWT), left ventricular end-systolic dimension (LVDs), and left ventricular end-diastolic dimension (LVDd) were measured by LV M-mode tracing. Percent fractional shortening (% FS) was calculated as % FS = [(LVDd − LVDs)/LVDd] × 100.

**Oxygen consumption measurements.** Measurements of respiration rates as oxygen consumption were conducted as described previously (13). Briefly, isolated mitochondria from a heart sample were suspended in respiration buffer (30 mM HEPES, 75 mM sucrose, 20 mM glucose, 5 mM potassium phosphate buffer [pH 7.1], 40 mM KCl, 0.5 mM EDTA, and 3 mM $MgCl_2$), and oxygen consumption of the isolated mitochondria was then measured at 30°C using a Clark electrode (Oxytherm; Hansatech Instruments) under consecutive administrations of oxidative substrates in the presence of 1 mM ADP: complex I-driven respiration, 5 mM glutamate and 5 mM malate; complex II-driven respiration, 10 mM succinate and 100 nM rotenone; complex IV-driven respiration, 10 mM ascorbate, 400 μM *N*,*N*,*N*′,*N*′-tetramethyl-*p*-phenylenediamine (TMPD), and 20 nM antimycin A. Each respiration rate was measured for 2 min starting 0.5 min after injection, and then the $O_2$ consumption rate was expressed as μM/μg/min.

**qPCR and RT-PCR.** DNA from mouse heart ventricle was extracted using a QIAamp DNA minikit (Qiagen) according to the manufacturer's instructions. A Kapa SYBR fast quantitative PCR (qPCR) kit was used for quantitative PCR with an ABI Prism 7000 sequence detection system (Applied Biosystems). The primer sets for amplification of mitochondrial DNA (part of the *COII* and $tRNA^{Lys}$ genes) and nuclear DNA (*Pecam*) fragments were as described previously (6, 28). Control heart ventricular

DNA was used to produce a standard curve for mtDNA and nuclear gene amplification. For reverse transcription-PCR (RT-PCR), single-stranded cDNA was generated from total RNA using the SuperScript first-strand synthesis system (Life Technologies). Each sample was amplified with specific primers for target genes, and PCR product quantities were normalized according to GAPDH expression. Primer sequences are available upon request.

**Cytochemical staining.** To assess reactive oxygen species (ROS) production, cells were cultured in a glass-bottom dish and incubated with MitoSOX (as an indicator of mitochondrial superoxide; Molecular Probes). Cells were coincubated with MitoTracker DeepRed 633 (Molecular Probes) to counterstain the mitochondria. After incubation for 10 min at 37°C, cells were rinsed briefly, and the average fluorescent intensity of all mitochondria in each cell was measured by microscopy.

**EM.** Heart sections were fixed with 2% paraformaldehyde and 2% glutaraldehyde in 0.1 M phosphate buffer (pH 7.4) at 4°C overnight, after which samples were analyzed by Tokai EM (13). Samples were rinsed three times with 0.1 M phosphate buffer (pH 7.4) for 30 min each, followed by postfixation with 2% osmium tetroxide in 0.1 M phosphate buffer (pH 7.4) at 4°C for 2 h. Fixed samples were dehydrated, infiltrated, embedded in Quetol-812 (Nisshin EM, Japan), and polymerized at 60°C for 48 h. The resin blocks were semithin sectioned into 1.5-μm sections with a glass knife using an ultramicrotome (Leica) and stained with 0.5% toluidine blue. The blocks were then ultrathin sectioned into 70-nm sections with a diamond knife using an ultramicrotome. Sections were placed on copper grids and stained with 2% uranyl acetate at room temperature for 15 min and then rinsed with distilled water, followed by secondary staining with lead stain solution (Sigma-Aldrich) at room temperature for 3 min. The grids were observed under a JEOL JEM-1200EX transmission electron microscope at an acceleration voltage of 80 kV.

## RESULTS

**Muscle-specific Drp1-deficient mice showed impaired postnatal cardiac function.** We previously reported that the mitochondrial fission factor Drp1 is essential for mouse development (7). However, besides the critical functions known in neuronal development (7–10), the functions of Drp1 in other developing tissues have been less well understood. Here, Drp1 protein levels in neonatal mouse tissues were examined by immunoblot analyses, which revealed strong expression in the brain and heart compared to other tissues or mouse embryonic fibroblasts (MEFs) (Fig. 1A). Combined with our previous report showing that Drp1 plays critical roles in the function of brain but not in that of MEFs (7), we speculate that Drp1 might have tissue-specific functions and that Drp1 might also have important roles in the heart. Note that the longer Drp1 protein in brain is reported to arise from an mRNA splice variant that contains a brain-specific insert (29). Next, Drp1 expression was subsequently analyzed during cardiac maturation (Fig. 1B and C). It is known that mouse cardiac myocytes stop proliferation around postnatal day 4 (P4), after which developmental hypertrophic growth leads to an increase in the diameter and mass of cardiomyocytes (30–32). As expected, the expression levels of mitochondrial protein Tom20 and myofibrillar protein α-actinin in heart at P7 were elevated until week 4 and were accompanied by hypertrophic growth (Fig. 1B). Inversely, the strong expression of Drp1 in the neonatal P7 heart was gradually reduced until week 4 (Fig. 1B and C), suggesting that Drp1 plays important roles in neonatal heart development.

To determine the role of mitochondrial fission in development and differentiation *in vivo*, we generated muscle-specific (MS) Drp1-KO mice. To selectively disrupt Drp1 in the heart and skeletal muscle, Drp1$^{flox/flox}$ mice were mated with muscle creatine kinase (Mck)-Cre transgenic mice (33, 34). Drp1 protein in the heart of MS-Drp1-KO (Drp1$^{flox/flox}$; Mck-Cre) mice was almost completely repressed at P1 (Fig. 1E). Because Drp1 was expressed in the KO heart at levels comparable with those of control mice at embryonic day 16.5 (E16.5) (Fig. 1D), the phenotypes seen in the KO mice were not caused by early developmental events in cardiogenesis. MS-Drp1-KO mice were born in the expected Mendelian ratio, but all pups died suddenly at P7 to P10 (Fig. 1G) after showing no suckling defects and no significant change in body weight (Fig. 1H and J). At P7, MS-Drp1-KO mice were found to have a dilated heart with relatively thin heart walls (Fig. 1I and L) but normal heart weight (Fig. 1K). Echocardiography revealed clear features of cardiac dysfunction, including an increase in the end-systolic dimension (0.85 mm in control to 1.64 mm in KO) and a decrease in the fractional shortening of the left ventricle (46.5% in control to 21.4% in KO) (Fig. 1N and O and Table 1). However, these hearts showed normal heartbeat cycles (Fig. 1M). We found that Drp1 protein was less repressed in skeletal muscle in MS-Drp1-KO mice (Fig. 1F), and we could not find clear abnormalities in the skeletal muscle or any other tissues (data not shown). Thus, the present findings show that Drp1 is essential for neonatal heart function.

**Drp1 deficiency exhibits myofibril disorganization in the neonatal heart.** Next, we observed ultrastructure during neonatal heart development by electron microscopy (EM). The P3 control heart had small spherical or thin tubular mitochondria that were loosely packed in the cytoplasm (Fig. 2A). In contrast, highly enlarged mitochondria were observed in the P3 Drp1-KO heart (Fig. 2A). In the P7 control heart, spherical mitochondria were aligned along developed myofibrils (Fig. 2A and B). However, mitochondria were aggregated in the Drp1-KO heart (Fig. 2A, middle panel, green) and were absent between myofibrils. The numerous thin tubular mitochondria in the KO heart were often connected to enlarged mitochondria (Fig. 2B). Enlarged mitochondria in the P7 KO heart had highly dense and stacked cristae (Fig. 2B). Furthermore, the P7 Drp1-KO heart had thinner, winding myofibrils and irregular Z lines (Fig. 2B, red arrowhead), suggesting severe disorganization. Immunofluorescent staining of F-actin in P7 KO heart cryosections also revealed thin, winding myofibril bundles with disrupted sarcomere structures (Fig. 2C).

In control P7 heart, one to several mitochondria were aligned beside a single sarcomere unit, consistent with the previous notion that mitochondrial distribution is synchronized with assembled sarcomere structures (18, 32, 35). In contrast, the size of the mitochondria varied in the KO heart, and the mitochondrial distribution did not correspond with the sarcomere units (Fig. 2A). Sarcoplasmic reticulum (SR) was often observed next to the mitochondria and Z lines in the sarcomere in the control P7 heart (Fig. 2B, blue arrowhead), as previously reported (35). However, we failed to find SR next to disorganized myofibrils in the KO heart (Fig. 2B). Thus, the higher-ordered structures composed of myofibrils, mitochondria, and SR were disrupted by the deficiency in mitochondrial fission.

**Impaired mitochondrial respiration in Drp1-KO heart.** Next, we further analyzed the role of mitochondrial fission in cardiomyocyte development. In heart sections, cell proliferation levels were comparable between the control and Drp1-KO heart when analyzed by immunostaining with the cell growth marker Ki-67 (Fig. 2D), as expected from the data indicating that Drp1-KO MEFs are viable (7). Myocardial differentiation also

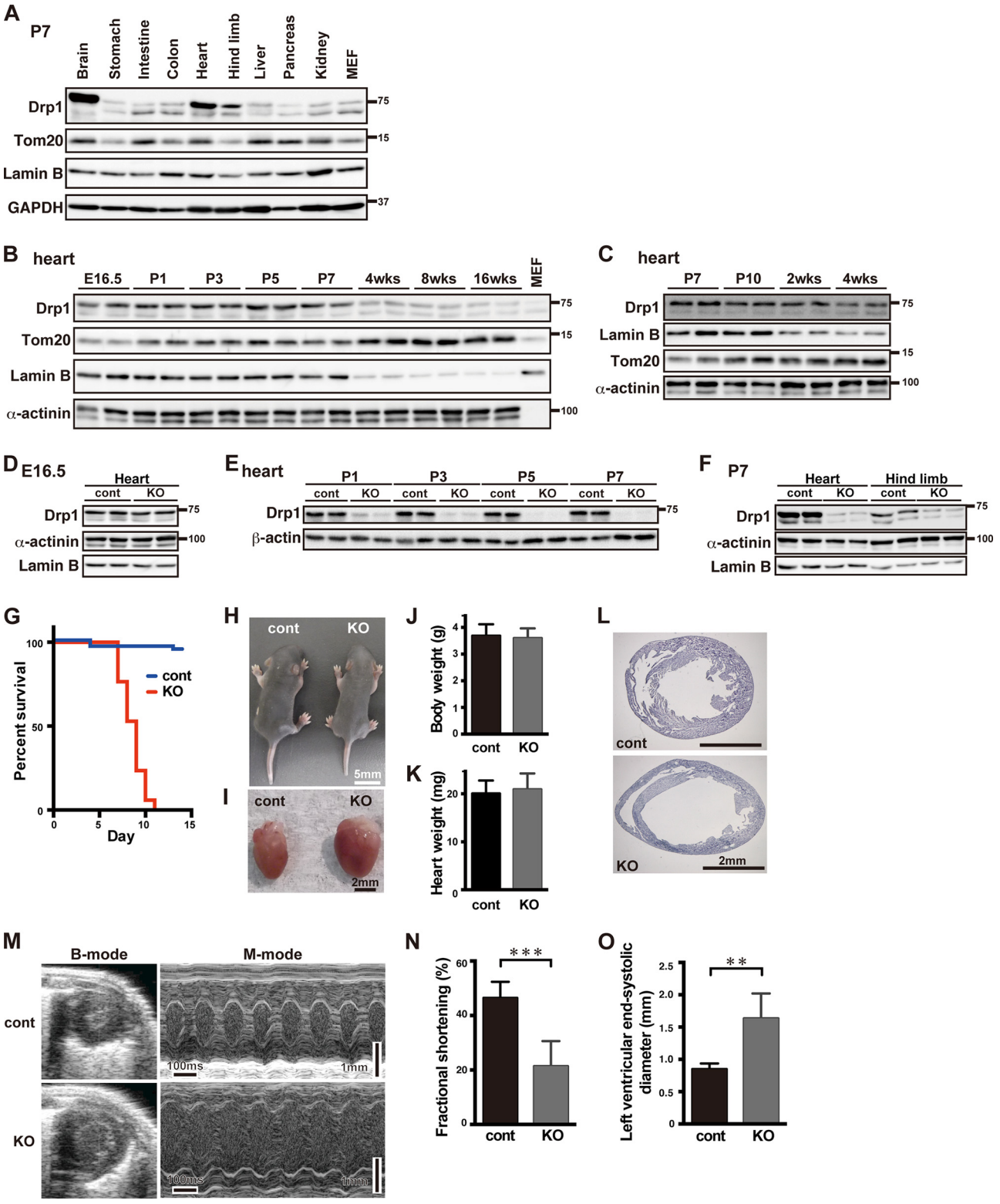


**FIG 1** Expression profiles of Drp1 and the phenotypes of muscle-specific (MS) Drp1-KO mice. (A) Immunoblot analysis of various tissues from a P7 control mouse. (B and C) Immunoblot analysis of heart protein samples from control mice at various developmental stages. (D and E) Deletion efficiency of Drp1 during embryonic (D) and postnatal (E) stages. (F) Immunoblot analysis of heart and hind limb protein samples at P7 from MS-Drp1-KO mice and a littermate control. (G) Survival curves of MS-Drp1-KO and control mice. (H and I) Images of P7 mice (H) and their hearts (I). (J and K) Mean weight of whole bodies (J) and the hearts (K) of P7 mice in control ($n = 9$) and MS-Drp1-KO ($n = 5$) mice. (L) Hematoxylin-eosin staining of a cryosection from a P7 heart. (M) Representative echocardiographic analysis showing B-mode and M-mode images. (N and O) Left ventricle fractional shortening (N) and left ventricular end-systolic diameter dimension (O) quantified by echocardiographic tracing in MS-Drp1-KO ($n = 4$) and control ($n = 6$) mice. Data are presented as the means ± standard deviations for all graphs. **, $P < 0.01$, and ***, $P < 0.001$, for KO compared with control. Molecular mass markers (kDa) are indicated to the right in panels A to F. Summarized echocardiographic measurement data are also shown in Table 1.

**TABLE 1** Summarized echocardiographic measurement data for MS-Drp1-KO and control mice[a,b]

| Genotype | Body wt (g) | IVST (mm) | PWT (mm) | LVDd (mm) | LVDs (mm) | % FS[c] |
|---|---|---|---|---|---|---|
| Control ($n = 6$) | 3.07 ± 0.69 | 0.48 ± 0.09 | 0.44 ± 0.02 | 1.60 ± 0.18 | 0.85 ± 0.08 | 46.48 ± 5.36 |
| MS-Drp1-KO ($n = 4$) | 3.14 ± 0.47 | 0.45 ± 0.03 | 0.40 ± 0.02* | 2.06 ± 0.29* | 1.64 ± 0.33** | 21.43 ± 7.98*** |

[a] Values are means ± standard deviations. The asterisks indicate significant differences (*, $P < 0.05$; **, $P < 0.01$; ***, $P < 0.001$).
[b] Abbreviations: IVST, interventricular septal thickness; PWT, left ventricular posterior wall thickness; LVDd, left ventricular end-diastolic diameter; LVDs, left ventricular end-systolic diameter.
[c] % FS = [(LVDd − LVDs)/LVDd] × 100.

seemed to proceed normally, because the cardiac developmental markers MYH6 and MYH7 showed comparable expression in RT-PCR (data not shown). The expression of succinate dehydrogenase (SDH), peroxisome proliferator-activated receptor gamma coactivator 1 (PGC1), and superoxide dismutase (SOD), as analyzed by RT-PCR (Fig. 3G), and Hsp60, Tom40, and Tim44, as analyzed by immunoblotting (Fig. 2F), were also normal. The P7 Drp1-KO cardiomyocytes exhibited a moderate induction of apoptosis (0.66%), slightly higher than that seen in control sections (0.32%) (Fig. 2E). In the Drp1-KO heart, the levels of the other mitochondrial fission proteins Mff and Fis1 and mitochondrial fusion proteins Mfn1/2 and L-OPA1 decreased, showing repression of mitochondrial dynamics (Fig. 2F). In addition, reduced levels of Parkin and increased levels of LC3-II suggest that mitochondrial autophagy might be enhanced in the Drp1-KO heart (Fig. 2G). These results suggest that Drp1 deficiency in cardiomyocytes affects mitochondrial dynamics and mitophagy, with less impact on differentiation, cell proliferation, cell death, and mitochondrial biogenesis.

To further examine heart dysfunction caused by mitochondrial fission deficiency, we assessed the mitochondrial respiratory function of the Drp1-KO heart. Histochemical staining of heart sections from P7 mice revealed that cytochrome *c* oxidase (COX) activity in MS-Drp1-KO mice was weaker than that of littermate control mice (Fig. 3A and B). Staining by SDH activity in KO mice was similar or partly diminished relative to control in heart sections (Fig. 3A). The pathology is different from that seen in mitochondrial fusion-deficient mice (6) and mitochondrial disease model mice (26, 34), in which SDH activity was upregulated in COX-deficient myotubules. We then measured the $O_2$ consumption of isolated heart mitochondria using a Clark electrode. Mitochondria from the P7 KO heart had a severely reduced $O_2$ consumption rate compared with those from a control littermate (Fig. 3C). These data were unexpected, because Drp1-KD HeLa cells (13) and KO MEFs (7) showed almost-normal respiration. Furthermore, immunoblot analysis revealed that protein levels of several respiratory chain subunits (NDUFB8 in complex I, UQCRC2 in complex III, and COX1 in complex IV [COX]) were reduced in the P7 KO heart but that of complex II (SDHB) was less affected (Fig. 3E and F). A similar observation was made in mtDNA expression-defective cells (13), suggesting that mtDNA expression is affected by Drp1 ablation in the heart.

Next, the mtDNA copy number was measured by qPCR analysis. The mtDNA/nuclear DNA (nDNA) ratio of control mice increased along with neonatal cardiac growth (Fig. 3D) (a 1.67-fold increase from P3 to P7). The normal mtDNA level of the P3 Drp1-KO heart failed to increase with neonatal growth (a 1.0-fold increase to P7), suggesting defective developmental growth of the KO heart. The mtDNA content of the P7 KO heart decreased to 0.57-fold that of the control. On the other hand, RT-PCR analysis revealed no significant differences in mitochondrial mRNA levels (Fig. 3G), suggesting that the reduction in mtDNA copy number per cell was not the main cause of respiratory deficiency and neonatal death in MS-Drp1-KO mice.

**Mitochondrial heterogeneity in the Drp1-KO mouse heart; mosaic respiratory deficiency and nucleoid aggregation.** To analyze the reason for the respiratory deficiency, we visualized the COX activity of each mitochondrion by COX-histochemical EM (COX-EM) (26). In control cardiomyocytes, mitochondria of a relatively homogeneous size were uniformly stained by COX activity (Fig. 4A, arrow). In Drp1-KO cardiomyocytes, most enlarged mitochondria were densely stained, while conversely, small mitochondria were stained to a lesser extent (Fig. 4A, arrowheads), suggesting mosaic respiration deficiency.

To further confirm the mitochondrial heterogeneity, we focused on mtDNA distribution, as we had recently demonstrated that mitochondrial fission is critical for the maintenance of nucleoid structures (13). Here, we investigated the structures and distribution of mtDNA nucleoids in mouse heart. When mtDNA in P7 KO heart sections was stained, the nucleoids were enlarged and aggregated, although many small nucleoids were observed in control heart sections (Fig. 4B). In the control heart, the distributions of nuclear genome-encoded mitochondrial protein Tom20 and the mtDNA-encoded COX subunit COX1 overlapped almost completely, and small nucleoids were dispersed across the mitochondria (Fig. 4C). In the Drp1-KO heart, COX1 accumulated locally in certain Tom20-positive structures in which nucleoids had also accumulated (Fig. 4C, arrow). In contrast, some Tom20-positive mitochondria showed faint COX1 staining (Fig. 4C, arrowhead). Nucleoids were rarely observed in the mitochondria that were weakly stained with COX1 (Fig. 4C, arrowheads). These results indicate that the clustering of local nucleoids in mitochondrial fission-deficient cardiomyocytes results in mitochondrial heterogeneity in respiratory subunits within single cardiomyocytes, which might be related to the mosaic deficiency of COX activity.

**Mitochondrial fission deficiency leads to abnormalities in hypertrophic growth, myofibril sarcomere formation, and mitochondrial heterogeneity.** For further analysis, we isolated cardiomyocytes from neonate control and MS-Drp1-KO mice for primary culture. In the control primary cultured cardiomyocytes, long and linear myofibrils with well-developed sarcomere structures aligned with mitochondria dispersed throughout the cytoplasm in a time-dependent manner (Fig. 5A, C, and D). On the other hand, cardiomyocytes from MS-Drp1-KO mice showed aggregated mitochondria in the perinuclear region and disorganized myofibrils (Fig. 5A and D), in addition to severe defects in hypertrophic cell growth (Fig. 5C and F). The number of well-organized Z lines observed as α-actinin bundles significantly decreased in Drp1-KO cells compared with control cells; instead, more small Z

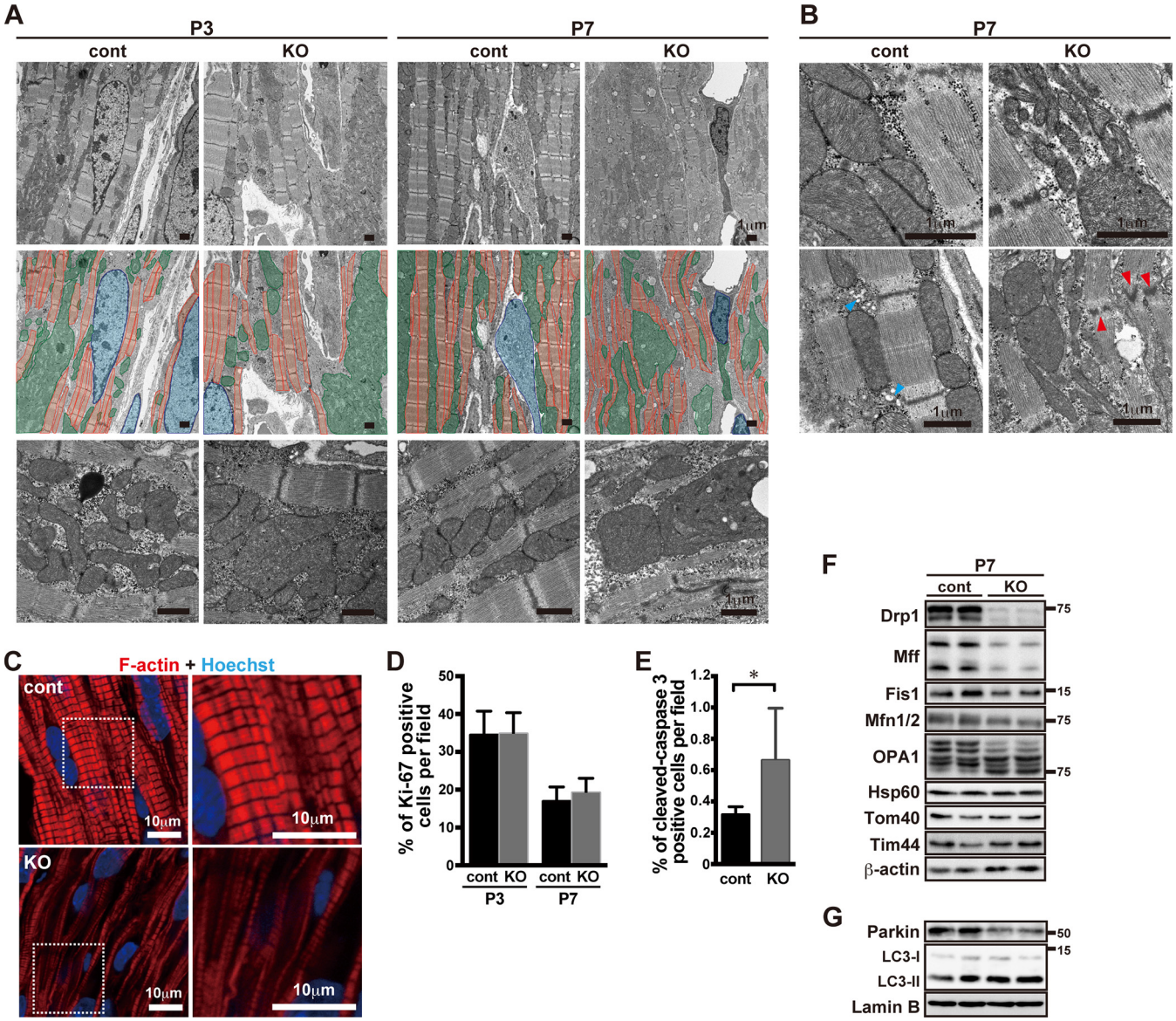


**FIG 2** Myofibril disorganization in the Drp1-KO heart. (A) Cardiomyocytes of control and MS-Drp1-KO mice during cardiac development were observed by electron microscopy. Middle panels show the distribution of nuclei (blue), mitochondria (green), and myofibrils (orange). (B) Magnified images of cardiomyocytes of control and MS-Drp1-KO mice at P7 observed by electron microscopy. Red arrowheads indicate disorganized sarcomeres, and blue arrowheads indicate SR structures. (C) Actin filaments were stained with rhodamine-phalloidin in cryosections from a P7 control and Drp1-KO heart and then were observed by confocal microscopy. (D) Cell proliferation was examined by immunostaining with Ki-67. The graph indicates the ratio of Ki-67-positive cells in the cross section. P3, control, $n = 8$; MS-Drp1-KO, $n = 5$; P7, control, $n = 5$; MS-Drp1-KO, $n = 6$. (E) Cell death in the P7 heart was evaluated by immunostaining with cleaved caspase-3. The graph indicates the ratio of cleaved caspase-3-positive-cells in the cross section. Control, $n = 5$; MS-Drp1-KO, $n = 8$. (F and G) Immunoblot analysis of mitochondrial biogenesis (F) and mitochondrial autophagy (G) in hearts from P7 control and Drp1-KO mice. Data are presented as the means ± standard deviations for all graphs. *, $P < 0.05$ for KO compared with control. Molecular mass markers (kDa) are indicated to the right in panels F and G.

bodies were observed (Fig. 5E and G). Mitochondrial ROS production in KO primary cultured cardiomyocytes was comparable to that in control cells (Fig. 5H and I), suggesting that the defective myofibril maturation was caused not by ROS production but by the mitochondrial distribution in primary cultured cardiomyocytes.

These phenotypes were also confirmed by RNAi knockdown (KD) of Drp1 (Fig. 6A to G). Repression of Drp1 protein levels was supported by immunoblotting and immunofluorescence microscopy (Fig. 6B and C), although there could be some cardiac fibroblast contamination in our immunoblotting samples.

Mfn1/2 DKO muscle and cardiomyocytes are reportedly defective in mtDNA maintenance and respiration, which causes muscle atrophy (6, 19, 20). We analyzed the role of mitochondrial fusion factors in primary cultured cardiomyocytes by RNAi KD. Cardiomyocytes with Mfn1/2 double KD (DKD) had highly fragmented mitochondria, as expected (Fig. 6D and E, magnified images), but

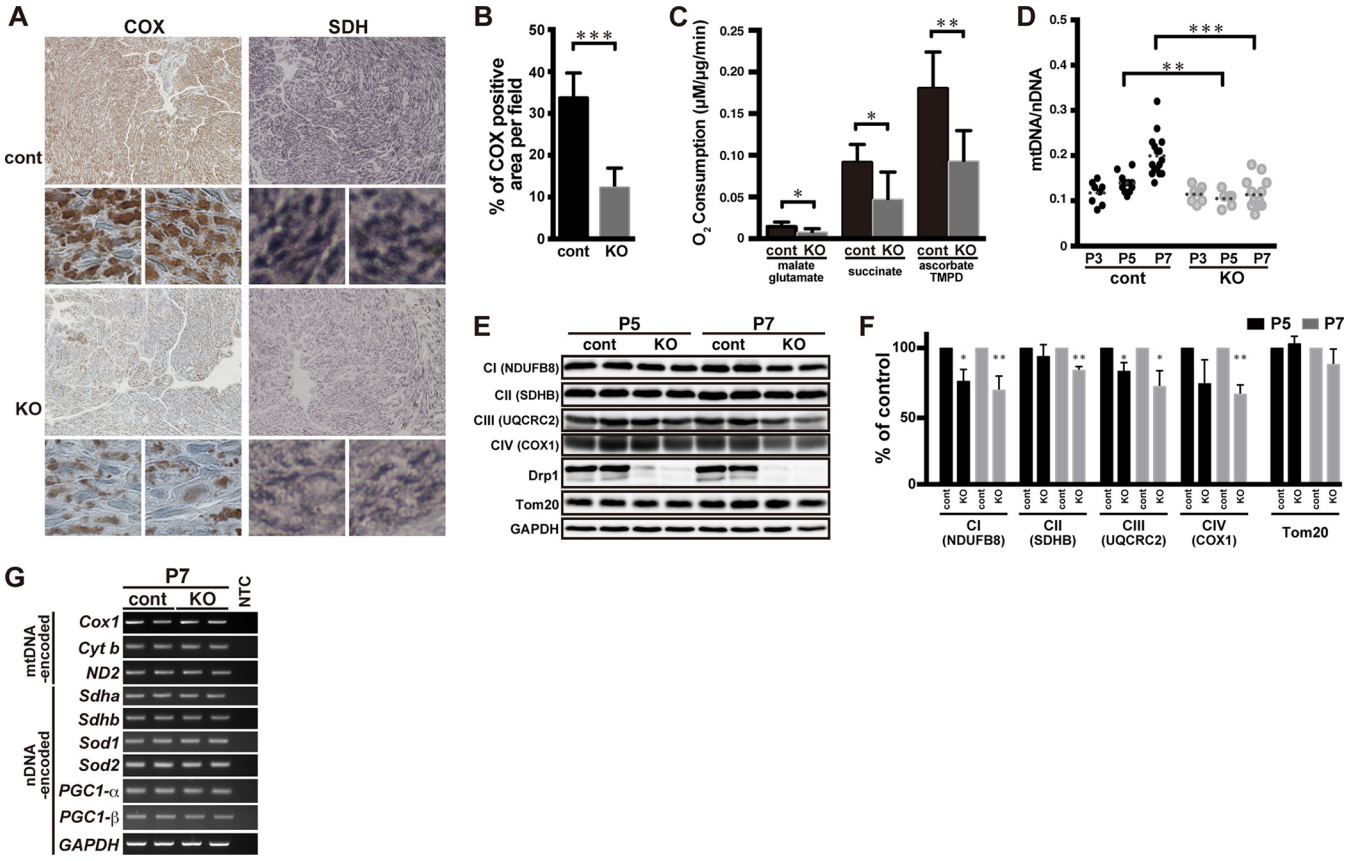


**FIG 3** Mitochondrial respiratory defect in Drp1-KO heart. (A) Histochemical staining for mitochondrial cytochrome *c* oxidase (COX) activity and succinate dehydrogenase (SDH) activity in heart samples from P7 mice. (B) ImageJ analysis was used to define the threshold and to measure the COX activity-positive area. Control, $n = 6$; MS-Drp1-KO, $n = 6$. (C) ADP-driven oxygen consumption by the isolated P7 mouse heart mitochondrial fraction. TMPD, *N*,*N*,*N*′,*N*′-tetramethyl-*p*-phenylenediamine. Control, $n = 5$; MS-Drp1-KO, $n = 7$. (D) mtDNA content quantified by qPCR, shown as the relative ratio of mtDNA to nDNA. Dashed horizontal bars are presented as means. (E) Immunoblot analysis of several respiratory subunits in heart samples from P5 and P7 mice. (F) Protein levels of respiratory chain subunits were quantified by ImageQuant TL. Four independent experiments with two littermate control and MS-Drp1-KO mouse hearts were performed. (G) RT-PCR analysis of the heart to determine mRNAs encoded by mtDNA and the nuclear genome. NTC, no-template negative control. Glyceraldehyde-3-phosphate dehydrogenase (GAPDH) was used to standardize reaction conditions and cDNA expression levels. Data are presented as the means ± standard deviations for all graphs. *, $P < 0.05$; **, $P < 0.01$; ***, $P < 0.001$.

exhibited hypertrophic growth similar to that of control cardiomyocytes (Fig. 6D, E, and F). Most mitochondria were associated with wider Z lines in control cardiomyocytes, whereas small fragmented mitochondria in the large cytoplasm of Mfn1/2 DKD cells were inefficiently associated with narrow dot-like Z bodies (Fig. 6E to G). Mitochondrial morphology is controlled by a balance between fusion and fission, and thus, defects introduced by ablation of a protein function that affects fusion are often rescued by inhibition of fission, or vice versa (36, 37). Thus, to address the importance of the balance between mitochondrial fusion and fission in these phenotypes, we performed triple KD of Mfn1/2 with Drp1. The cell area of Drp1 KD cardiomyocytes was rescued by further Mfn1/2 KD (Fig. 6D and F). The number of matured α-actinin bands was not rescued by Mfn1/2 KD in fission-deficient cells (Fig. 6E and G); however, small Z bodies were increased (Fig. 6G; Drp1 KD, 539.7 ± 233.3 per cell; triple KD, 876.3 ± 429.9 per cell). These results showed that impairment of mitochondrial fusion partly rescued the severe phenotypes seen in the fission-deficient cells, which suggests the importance of balanced fusion/fission for cardiac hypertrophy. Thus, mitochondrial dynamics might be important for myofibril formation during cardiomyocyte growth. Next, we further analyzed the effect of Drp1 KD on well-grown primary cardiomyocytes (Fig. 6H). Cardiomyocytes were cultured for 4 days after isolation, and were then treated with Drp1 siRNA. The RNAi treatment again caused Drp1 repression and mitochondrial tubulation in matured cardiomyocytes (Fig. 6I); however, both cell area (Fig. 6J and K) and sarcomere formation (Fig. 6J and L) were affected little by Drp1 ablation relative to observations in growing cardiomyocytes (Fig. 6A to G). This result supports our conclusion that Drp1 might play a critical role in developmental cardiomyocyte hypertrophy in mice.

Next, the distribution of mtDNA in primary cultured cardiomyocytes was examined by immunofluorescence microscopy. In primary cultured cardiomyocytes from MS-Drp1-KO mice, COX1 subunit and clustered enlarged nucleoids accumulated in mito-bulbs in immature cardiomyocytes (Fig. 7A), as can be seen in heart sections. Both heterogeneity in respiratory activity and that in mtDNA distribution were also observed in the cultured cardiomyocytes (Fig. 7B). COX activity was concentrated in the nucleoid-enriched mito-bulbs, even though the mitochondrial network had less COX activity. Thus, these findings show that during cardiomyocyte growth, mitochondrial fission mediates

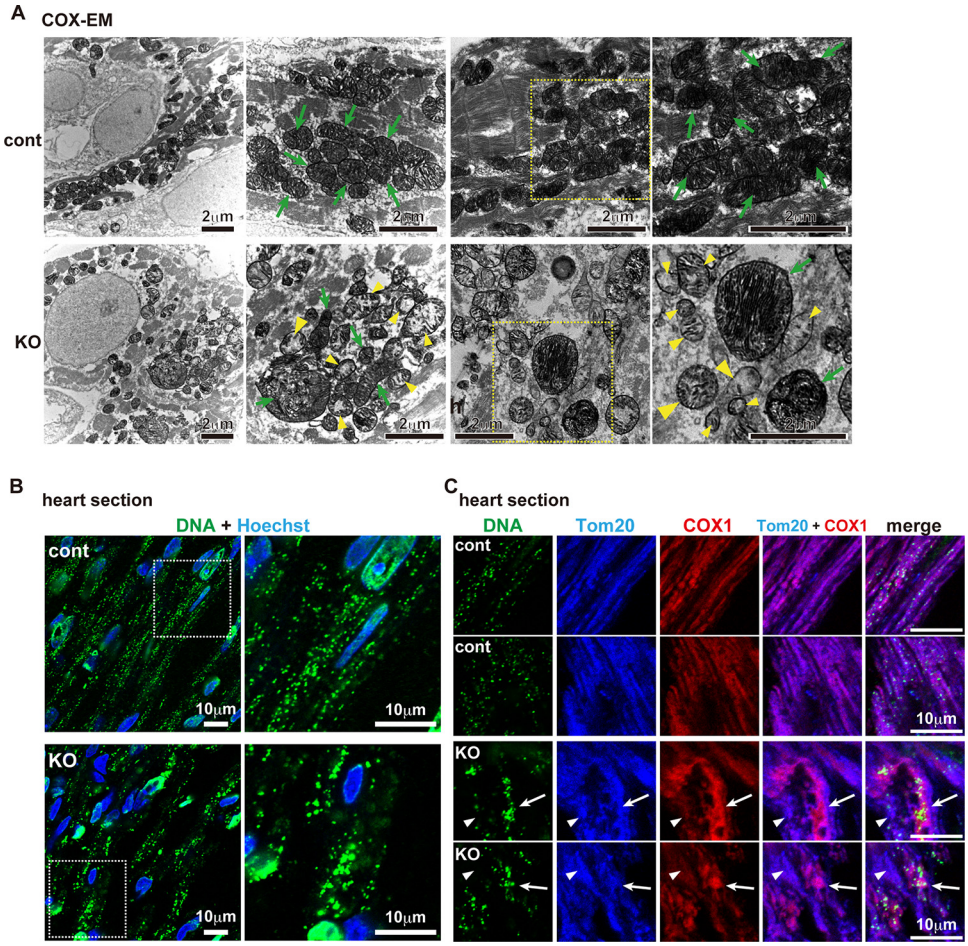


**FIG 4** Heterogeneity of respiration and mtDNA nucleoid distribution in Drp1-KO heart. (A) Electron microscopic analysis of COX activity in P7 control and MS-Drp1-KO heart sections. Arrows indicate mitochondria retaining COX activity, and arrowheads indicate COX-deficient mitochondria. (B) Anti-DNA (green) immunofluorescence staining of mtDNA nucleoids in cryosections from P7 control and MS-Drp1-KO mouse hearts observed by confocal microscopy. Nuclei were stained with Hoechst stain (blue). (C) Mitochondrial heterogeneity was confirmed by triple staining with nucleoid-specific stain (green), nuclear genome-encoded Tom20 (blue), and mtDNA-encoded respiratory subunit COX1 (red). Arrows indicate COX1-stained mitochondria that are accumulating, accompanied by nucleoid clustering. Arrowheads indicate Tom20-positive mitochondria with less COX1 staining.

dispersion of homogeneously active mitochondria, which could support myofibril formation.

## DISCUSSION

In cardiomyocytes, myofibrils are tightly associated with mitochondria to form synchronized sarcomere structures. Here, we report the roles of mitochondrial fission in cardiomyocyte development *in vivo* and clarify that local accumulation of mitochondria with aggregated mtDNA nucleoids in the substantial, developed cytoplasm resulted in immature myofibril formation, respiratory deficiency, and heart dysfunction in MS-Drp1-KO mice.

It is well known that impaired mitochondrial fission enhances the intermixing of mitochondria by countering mitochondrial fusion (6, 38). However, we report here that *in vivo* Drp1 ablation in cardiomyocytes leads to heterogeneity of mitochondria and respiratory deficiency. As we reported previously, defective mitochondrial fission leads to clustering of mtDNA nucleoids, resulting in a decreased number of nucleoids in each cell (13). The respiration deficiency in the Drp1-KO heart seems to be related to the mtDNA clustering. Sparse distribution of nucleoids in the large cardiomyocyte cytoplasm might lead to an insufficient energy supply for cardiomyocyte growth. Thus, our findings show that mitochondrial fission supports dispersed nucleoids throughout cardiomyocytes for maintaining proper distribution of active mitochondria during postnatal maturation of the heart.

The fact that conventional Drp1-KO ($Drp1^{-/-}$) mice with normal heart structures (7) exhibit embryonic lethality at around E12.5 suggests that there are stage-specific roles for Drp1 in heart development. Respiration deficiency in the Drp1-ablated heart is likely a tissue-specific effect, because Drp1 KD HeLa cells (13) and KO MEFs (7) showed almost-normal respiration. Balanced transcription and translation from both the nuclear and mitochondrial genomes are necessary for the assembly of a functional respiratory complex. Although mitochondrial transcripts encoding respiratory subunits were expressed normally in Drp1-KO hearts, impaired assembly of the respiratory complex led to destabilization of these subunits. We speculate that respiratory subunits encoded in mtDNA are locally expressed in enlarged mitochondria, mito-bulbs, and that they are less mobile and become fixed in large

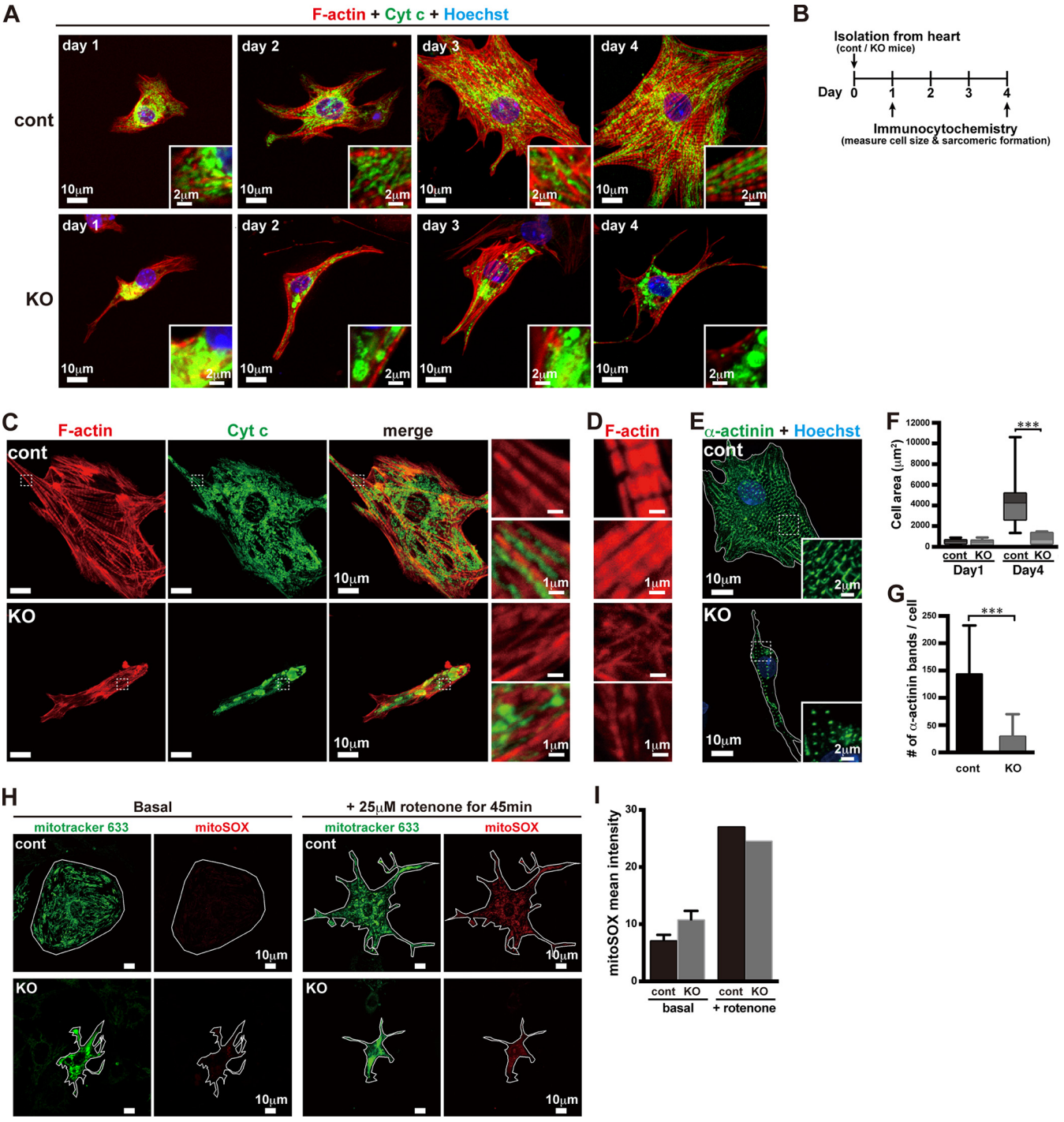


**FIG 5** Suppression of hypertrophic growth and sarcomere formation in Drp1-KO cardiomyocytes. (A) Primary cultured cardiomyocytes from control mice and MS-Drp1-KO mice were cultured for 1, 2, 3, or 4 days and stained with anti-cytochrome *c* (green), rhodamine-phalloidin (red), and Hoechst stain (blue) and then observed by confocal microscopy. (B) Schematic diagram for the time course of the experiment (C to G). (C) Primary cultured cardiomyocytes from control and MS-Drp1-KO mice were cultured for 4 days, stained with anti-cytochrome *c* (green) and rhodamine-phalloidin (red), and then observed by confocal microscopy. (D) Magnified images showing the sarcomere structures. (E) Z lines immunostained by anti-α-actinin. (F and G) Cell surface area and Z line number measurement were calculated using Zeiss Zen 2010LSM software. (F) Box-and-whisker plots of the cardiomyocyte surface area after culturing for 1 or 4 days. (G) Quantification of Z line number in cardiomyocytes after culturing for 4 days. (H and I) Representative image of staining with fluorescent dye mitoSOX to monitor mitochondrial ROS, with counterstaining by MitoTracker DeepRed 633 (H). Rotenone was used as the positive control. The fluorescence ratio of the mitoSOX was quantified by confocal microscopy (I). Data are presented as the means ± standard deviations for bar graphs. ***, $P < 0.001$.

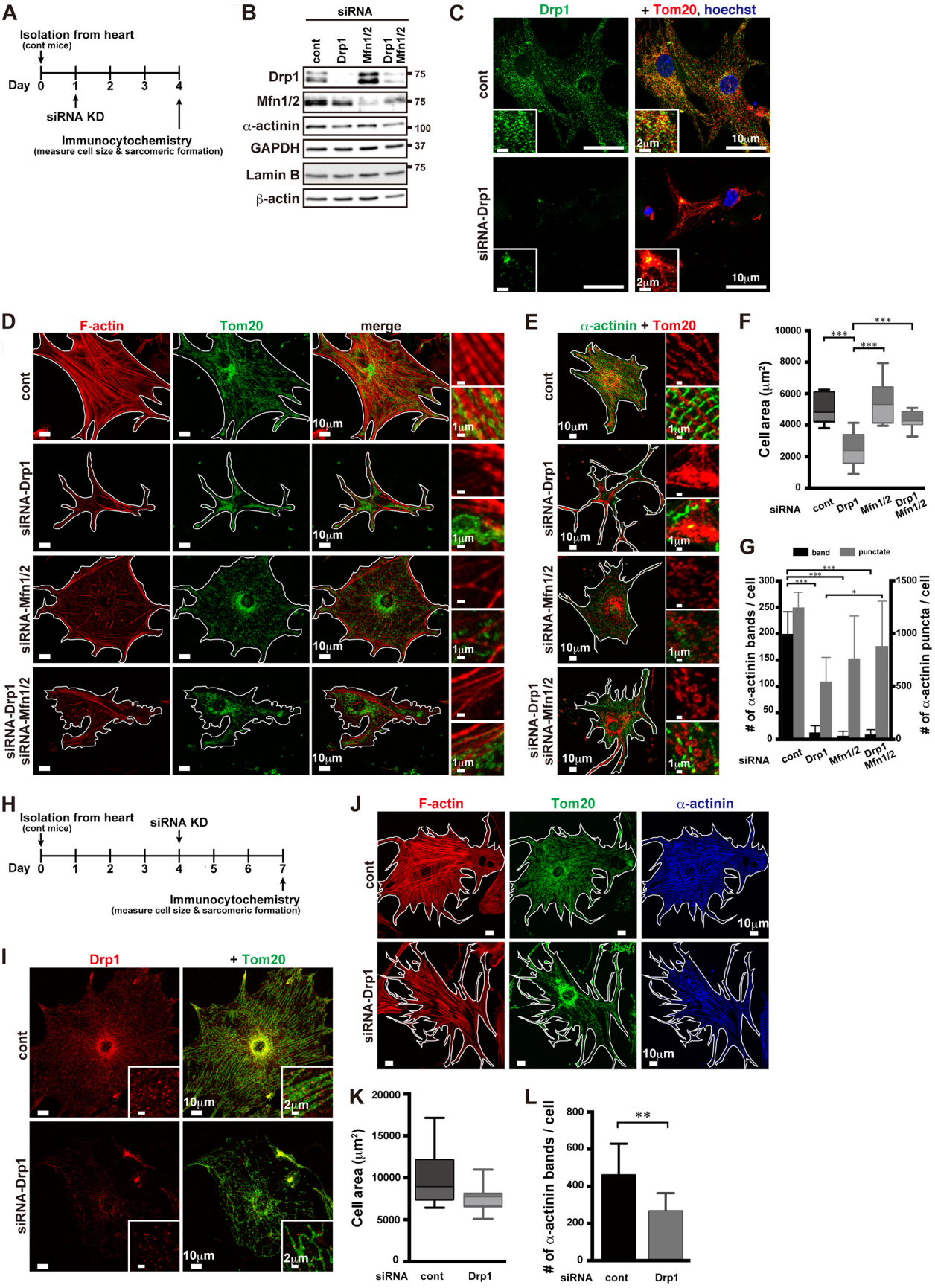
A
Isolation from heart
(cont mice)
Day 0 1 2 3 4
siRNA KD
Immunocytochemistry
(measure cell size & sarcomeric formation)
B
siRNA
cont
Drp1
Mfn1/2
Drp1 Mfn1/2
Drp1
Mfn1/2
α-actinin
GAPDH
Lamin B
β-actin
75
75
100
37
75
C
Drp1
+ Tom20, hoechst
cont
siRNA-Drp1
2μm
10μm
D
F-actin
Tom20
merge
cont
siRNA-Drp1
siRNA-Mfn1/2
siRNA-Drp1 siRNA-Mfn1/2
10μm
1μm
E
α-actinin + Tom20
F
Cell area (μm²)
siRNA cont Drp1 Mfn1/2 Drp1 Mfn1/2
***
G
band
punctate
# of α-actinin bands / cell
# of α-actinin puncta / cell
H
Isolation from heart
(cont mice)
siRNA KD
Day 0 1 2 3 4 5 6 7
Immunocytochemistry
(measure cell size & sarcomeric formation)
I
Drp1
+ Tom20
J
F-actin
Tom20
α-actinin
K
Cell area (μm²)
siRNA cont Drp1
L
# of α-actinin bands / cell
**

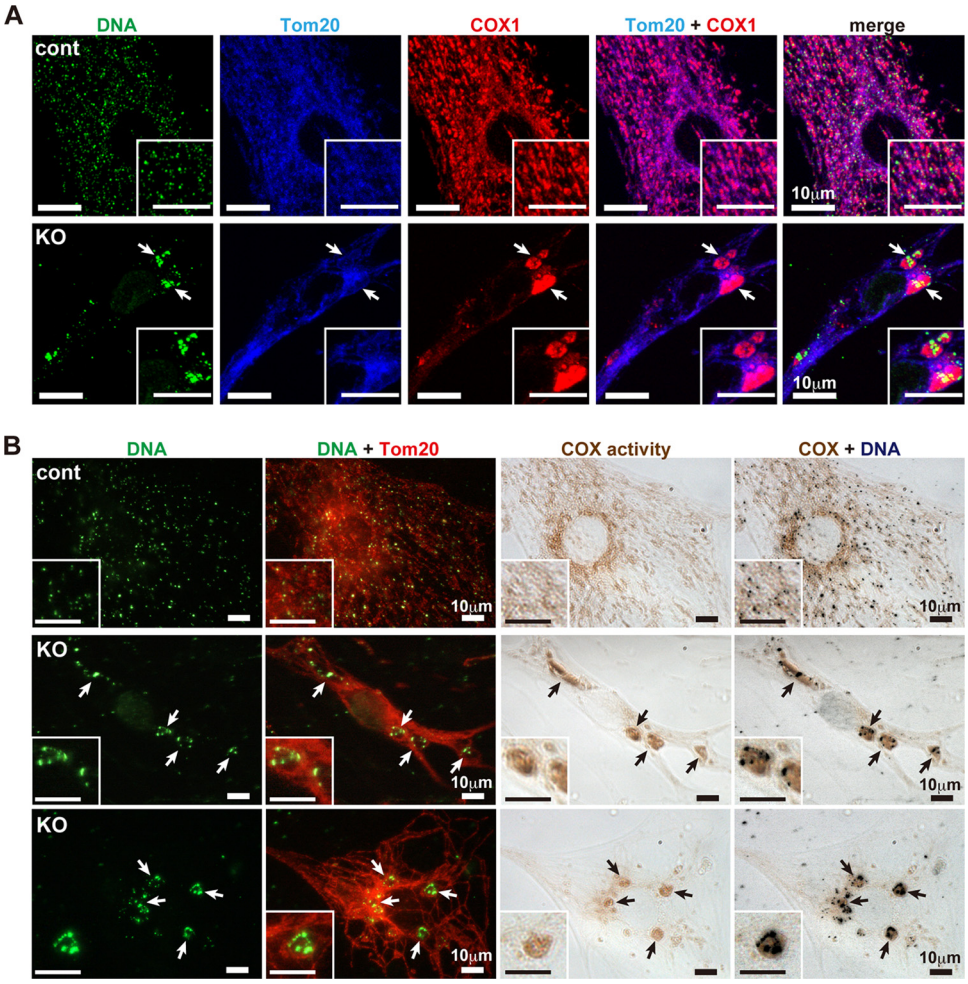


**FIG 7** mtDNA nucleoid clustering accompanied by heterogeneity in COX activity in Drp1-KO cardiomyocytes. (A) Primary cultured cardiomyocytes stained with anti-DNA antibody (green), anti-Tom20 (blue), and anti-COX1 (red). (B) Primary cultured cardiomyocytes stained by anti-DNA antibody (green) and anti-Tom20 (red) and COX activity visualized by 3,3′-diaminobenzidine (brown).

cardiomyocytes (16). This in turn compromises their uniform distribution, their assembly with the nucleus-encoded subunits, and the stability of the respiratory complex in cardiomyocyte mitochondria. Thus, mitochondrial fission appears to mediate distribution of mtDNA into many isolated, immobile mitochondria in cardiomyocytes, consequently enhancing total respiratory levels. It is possible that mitochondrial fusion also becomes involved in maintenance of nucleoid structures in the heart and leads to respiratory deficiency (19, 20), although further analysis is needed to test this hypothesis.

The molecular details of nucleoid formation remain unclear. Several recent reports showed that mitochondrial fission is critical for nucleoid morphogenesis in cultured mammalian cells (13) and in yeast (39), and we have also reported that the enlarged nucleoids in HeLa cells compromised release of cytochrome *c* from dense cristae under proapoptotic conditions (13). However, the *in vivo* functions of nucleoids remain unknown. The anticancer drug doxorubicin was previously reported to cause heart failure by inducing respiratory deficiency in addition to nucleoid clustering (40). It is therefore possible that nucleoid structure and distribution become altered under certain pathological conditions, including not only heart fail-

**FIG 6** Regulation of hypertrophic growth and sarcomere formation through mitochondrial dynamics in primary cultured cardiomyocytes. (A) Schematic diagram for time course of experiment (D to G). (B and C) Confirmation of knockdown efficiency in isolated cells from heart by immunoblotting (B) and immunofluorescence staining (C). Molecular mass markers (kDa) are indicated to the right in panel B. (D to G) Primary cultured cardiomyocytes were treated with siRNA against Drp1, Mfn1/Mfn2, or Drp1/Mfn1/Mfn2 for 3 days and then stained as indicated. Confocal images are shown in panels D and E. Quantification of cardiomyocyte surface area (F) and matured Z line (left axis) and measurement of small Z body number (right axis) (G) were done using Zeiss ZEN 2010LSM software. (H) Schematic for the time course of the experiment (J to L). Grown primary cultured cardiomyocytes were treated for 3 days with siRNA against Drp1 and then stained as indicated. (I) Confirmation of knockdown efficiency in cardiomyocytes by immunofluorescence staining. (J) Confocal images were triple stained with anti-Tom20 (green), rhodamine-phalloidin (red), and anti-α-actinin (blue). (K) Full-grown cardiomyocyte surface area quantified as described for panel F. (L) Matured Z line quantified as described for panel G. Data are presented as the means ± standard deviations for bar graphs. *, $P < 0.05$; **, $P < 0.01$; ***, $P < 0.001$.

ure but also other pathologies such as neurodegenerative and metabolic diseases. Further extensive analysis of nucleoid distribution in mammalian tissues will help clarify the pathophysiological roles of nucleoid distribution-controlled mitochondrial membrane dynamics. The results of this study offer clarification of the fundamental features of mitochondrial dynamics during heart development and in various cellular processes and diseases related to mitochondrial function.

## ACKNOWLEDGMENTS

We thank C. Ronald Kahn (Harvard Medical School) for supplying Mck-Cre Tg mice.

This work was supported by the Funding Program for Next-Generation World-Leading Researchers (N.I.), the Takeda Science Foundation (N.I.), and JSPS KAKENHI grant number 24770133 (T.I.).

We declare no competing financial interests.

## REFERENCES

1. **Ishihara N, Otera H, Oka T, Mihara K.** 2013. Regulation and physiologic functions of GTPases in mitochondrial fusion and fission in mammals. Antioxid Redox Signal **19:**389–399. http://dx.doi.org/10.1089/ars.2012.4830.
2. **McBride HM, Neuspiel M, Wasiak S.** 2006. Mitochondria: more than just a powerhouse. Curr Biol **16:**R551–R560. http://dx.doi.org/10.1016/j.cub.2006.06.054.
3. **Nunnari J, Suomalainen A.** 2012. Mitochondria: in sickness and in health. Cell **148:**1145–1159. http://dx.doi.org/10.1016/j.cell.2012.02.035.
4. **Chen H, Chomyn A, Chan DC.** 2005. Disruption of fusion results in mitochondrial heterogeneity and dysfunction. J Biol Chem **280:**26185–26192. http://dx.doi.org/10.1074/jbc.M503062200.
5. **Chen H, McCaffery JM, Chan DC.** 2007. Mitochondrial fusion protects against neurodegeneration in the cerebellum. Cell **130:**548–562. http://dx.doi.org/10.1016/j.cell.2007.06.026.
6. **Chen H, Vermulst M, Wang YE, Chomyn A, Prolla TA, McCaffery JM, Chan DC.** 2010. Mitochondrial fusion is required for mtDNA stability in skeletal muscle and tolerance of mtDNA mutations. Cell **141:**280–289. http://dx.doi.org/10.1016/j.cell.2010.02.026.
7. **Ishihara N, Nomura M, Jofuku A, Kato H, Suzuki SO, Masuda K, Otera H, Nakanishi Y, Nonaka I, Goto Y, Taguchi N, Morinaga H, Maeda M, Takayanagi R, Yokota S, Mihara K.** 2009. Mitochondrial fission factor Drp1 is essential for embryonic development and synapse formation in mice. Nat Cell Biol **11:**958–966. http://dx.doi.org/10.1038/ncb1907.
8. **Kageyama Y, Zhang Z, Roda R, Fukaya M, Wakabayashi J, Wakabayashi N, Kensler TW, Reddy PH, Iijima M, Sesaki H.** 2012. Mitochondrial division ensures the survival of postmitotic neurons by suppressing oxidative damage. J Cell Biol **197:**535–551. http://dx.doi.org/10.1083/jcb.201110034.
9. **Wakabayashi J, Zhang Z, Wakabayashi N, Tamura Y, Fukaya M, Kensler TW, Iijima M, Sesaki H.** 2009. The dynamin-related GTPase Drp1 is required for embryonic and brain development in mice. J Cell Biol **186:**805–816. http://dx.doi.org/10.1083/jcb.200903065.
10. **Waterham HR, Koster J, van Roermund CW, Mooyer PA, Wanders RJ, Leonard JV.** 2007. A lethal defect of mitochondrial and peroxisomal fission. N Engl J Med **356:**1736–1741. http://dx.doi.org/10.1056/NEJMoa064436.
11. **Holt IJ, He J, Mao CC, Boyd-Kirkup JD, Martinsson P, Sembongi H, Reyes A, Spelbrink JN.** 2007. Mammalian mitochondrial nucleoids: organizing an independently minded genome. Mitochondrion **7:**311–321. http://dx.doi.org/10.1016/j.mito.2007.06.004.
12. **Kang D, Kim SH, Hamasaki N.** 2007. Mitochondrial transcription factor A (TFAM): roles in maintenance of mtDNA and cellular functions. Mitochondrion **7:**39–44. http://dx.doi.org/10.1016/j.mito.2006.11.017.
13. **Ban-Ishihara R, Ishihara T, Sasaki N, Mihara K, Ishihara N.** 2013. Dynamics of nucleoid structure regulated by mitochondrial fission contributes to cristae reformation and release of cytochrome c. Proc Natl Acad Sci U S A **110:**11863–11868. http://dx.doi.org/10.1073/pnas.1301951110.
14. **Dorn GW, II.** 2013. Mitochondrial dynamics in heart disease. Biochim Biophys Acta **1833:**233–241. http://dx.doi.org/10.1016/j.bbamcr.2012.03.008.
15. **Olson EN.** 2004. A decade of discoveries in cardiac biology. Nat Med **10:**467–474. http://dx.doi.org/10.1038/nm0504-467.
16. **Huang X, Sun L, Ji S, Zhao T, Zhang W, Xu J, Zhang J, Wang Y, Wang X, Franzini-Armstrong C, Zheng M, Cheng H.** 2013. Kissing and nanotunneling mediate intermitochondrial communication in the heart. Proc Natl Acad Sci U S A **110:**2846–2851. http://dx.doi.org/10.1073/pnas.1300741110.
17. **Pham AH, McCaffery JM, Chan DC.** 2012. Mouse lines with photo-activatable mitochondria to study mitochondrial dynamics. Genesis **50:**833–843. http://dx.doi.org/10.1002/dvg.22050.
18. **Piquereau J, Caffin F, Novotova M, Lemaire C, Veksler V, Garnier A, Ventura-Clapier R, Joubert F.** 2013. Mitochondrial dynamics in the adult cardiomyocytes: which roles for a highly specialized cell? Front Physiol **4:**102. http://dx.doi.org/10.3389/fphys.2013.00102.
19. **Chen Y, Liu Y, Dorn GW, II.** 2011. Mitochondrial fusion is essential for organelle function and cardiac homeostasis. Circ Res **109:**1327–1331. http://dx.doi.org/10.1161/CIRCRESAHA.111.258723.
20. **Papanicolaou KN, Kikuchi R, Ngoh GA, Coughlan KA, Dominguez I, Stanley WC, Walsh K.** 2012. Mitofusins 1 and 2 are essential for postnatal metabolic remodeling in heart. Circ Res **111:**1012–1026. http://dx.doi.org/10.1161/CIRCRESAHA.112.274142.
21. **Chen Y, Dorn GW, II.** 2013. PINK1-phosphorylated mitofusin 2 is a Parkin receptor for culling damaged mitochondria. Science **340:**471–475. http://dx.doi.org/10.1126/science.1231031.
22. **Ashrafian H, Docherty L, Leo V, Towlson C, Neilan M, Steeples V, Lygate CA, Hough T, Townsend S, Williams D, Wells S, Norris D, Glyn-Jones S, Land J, Barbaric I, Lalanne Z, Denny P, Szumska D, Bhattacharya S, Griffin JL, Hargreaves I, Fernandez-Fuentes N, Cheeseman M, Watkins H, Dear TN.** 2010. A mutation in the mitochondrial fission gene Dnm1l leads to cardiomyopathy. PLoS Genet **6:**e1001000. http://dx.doi.org/10.1371/journal.pgen.1001000.
23. **Ong SB, Subrayan S, Lim SY, Yellon DM, Davidson SM, Hausenloy DJ.** 2010. Inhibiting mitochondrial fission protects the heart against ischemia/reperfusion injury. Circulation **121:**2012–2022. http://dx.doi.org/10.1161/CIRCULATIONAHA.109.906610.
24. **Sharp WW, Fang YH, Han M, Zhang HJ, Hong Z, Banathy A, Morrow E, Ryan JJ, Archer SL.** 2014. Dynamin-related protein 1 (Drp1)-mediated diastolic dysfunction in myocardial ischemia-reperfusion injury: therapeutic benefits of Drp1 inhibition to reduce mitochondrial fission. FASEB J **28:**316–326. http://dx.doi.org/10.1096/fj.12-226225.
25. **Sreejit P, Kumar S, Verma RS.** 2008. An improved protocol for primary culture of cardiomyocyte from neonatal mice. In Vitro Cell Dev Biol Anim **44:**45–50. http://dx.doi.org/10.1007/s11626-007-9079-4.
26. **Nakada K, Inoue K, Ono T, Isobe K, Ogura A, Goto YI, Nonaka I, Hayashi JI.** 2001. Inter-mitochondrial complementation: mitochondria-specific system preventing mice from expression of disease phenotypes by mutant mtDNA. Nat Med **7:**934–940. http://dx.doi.org/10.1038/90976.
27. **Oba T, Yasukawa H, Hoshijima M, Sasaki K, Futamata N, Fukui D, Mawatari K, Nagata T, Kyogoku S, Ohshima H, Minami T, Nakamura K, Kang D, Yajima T, Knowlton KU, Imaizumi T.** 2012. Cardiac-specific deletion of SOCS-3 prevents development of left ventricular remodeling after acute myocardial infarction. J Am Coll Cardiol **59:**838–852. http://dx.doi.org/10.1016/j.jacc.2011.10.887.
28. **Shitara H, Hayashi JI, Takahama S, Kaneda H, Yonekawa H.** 1998. Maternal inheritance of mouse mtDNA in interspecific hybrids: segregation of the leaked paternal mtDNA followed by the prevention of subsequent paternal leakage. Genetics **148:**851–857.
29. **Smirnova E, Shurland DL, Ryazantsev SN, van der Bliek AM.** 1998. A human dynamin-related protein controls the distribution of mitochondria. J Cell Biol **143:**351–358. http://dx.doi.org/10.1083/jcb.143.2.351.
30. **Leu M, Ehler E, Perriard JC.** 2001. Characterisation of postnatal growth of the murine heart. Anat Embryol **204:**217–224. http://dx.doi.org/10.1007/s004290100206.
31. **Li F, Wang X, Capasso JM, Gerdes AM.** 1996. Rapid transition of cardiac myocytes from hyperplasia to hypertrophy during postnatal development. J Mol Cell Cardiol **28:**1737–1746. http://dx.doi.org/10.1006/jmcc.1996.0163.
32. **Piquereau J, Novotova M, Fortin D, Garnier A, Ventura-Clapier R, Veksler V, Joubert F.** 2010. Postnatal development of mouse heart: formation of energetic microdomains. J Physiol **588:**2443–2454. http://dx.doi.org/10.1113/jphysiol.2010.189670.
33. **Bruning JC, Michael MD, Winnay JN, Hayashi T, Horsch D, Accili D, Goodyear LJ, Kahn CR.** 1998. A muscle-specific insulin receptor knockout exhibits features of the metabolic syndrome of NIDDM without alter-

ing glucose tolerance. Mol Cell **2:**559–569. http://dx.doi.org/10.1016/S1097-2765(00)80155-0.
34. **Wang J, Wilhelmsson H, Graff C, Li H, Oldfors A, Rustin P, Bruning JC, Kahn CR, Clayton DA, Barsh GS, Thoren P, Larsson NG.** 1999. Dilated cardiomyopathy and atrioventricular conduction blocks induced by heart-specific inactivation of mitochondrial DNA gene expression. Nat Genet **21:**133–137. http://dx.doi.org/10.1038/5089.
35. **Sheldon CA, Friedman WF, Sybers HD.** 1976. Scanning electron microscopy of fetal and neonatal lamb cardiac cells. J Mol Cell Cardiol **8:**853–862. http://dx.doi.org/10.1016/0022-2828(76)90068-7.
36. **Lee YJ, Jeong SY, Karbowski M, Smith CL, Youle RJ.** 2004. Roles of the mammalian mitochondrial fission and fusion mediators Fis1, Drp1, and Opa1 in apoptosis. Mol Biol Cell **15:**5001–5011. http://dx.doi.org/10.1091/mbc.E04-04-0294.
37. **Sesaki H, Jensen RE.** 1999. Division versus fusion: Dnm1p and Fzo1p antagonistically regulate mitochondrial shape. J Cell Biol **147:**699–706. http://dx.doi.org/10.1083/jcb.147.4.699.
38. **Chen H, Detmer SA, Ewald AJ, Griffin EE, Fraser SE, Chan DC.** 2003. Mitofusins Mfn1 and Mfn2 coordinately regulate mitochondrial fusion and are essential for embryonic development. J Cell Biol **160:**189–200. http://dx.doi.org/10.1083/jcb.200211046.
39. **Murley A, Lackner LL, Osman C, West M, Voeltz GK, Walter P, Nunnari J.** 2013. ER-associated mitochondrial division links the distribution of mitochondria and mitochondrial DNA in yeast. eLife **2:**e00422. http://dx.doi.org/10.7554/eLife.00422.
40. **Ashley N, Poulton J.** 2009. Anticancer DNA intercalators cause p53-dependent mitochondrial DNA nucleoid re-modelling. Oncogene **28:**3880–3891. http://dx.doi.org/10.1038/onc.2009.242.